International Forum on Aeroelasticity and Structural Dynamics
IFASD 2024
17-21 June 2024, The Hague, The Netherlands

ANALYSIS OF LINEARIZED MOTION- AND GUST-INDUCED AIRLOADS WITH A NEXT-GENERATION COMPUTATIONAL FLUID DYNAMICS SOLVER

Christoph Kaiser[1], **David Quero**[1], **Jens Nitzsche**[1], **Bernd Stickan**[2]

[1]DLR (German Aerospace Center), Institute of Aeroelasticity
Bunsenstr. 10, 37073 Göttingen, Germany
christoph.kaiser@dlr.de
david.queromartin@dlr.de
jens.nitzsche@dlr.de

[2]Airbus Operations GmbH
Airbus-Allee 1, 28199 Bremen, Germany
bernd.b.stickan@airbus.com

Keywords: aeroelasticity, linearized CFD, LFD solver, system identification, pulse, gust, flutter

Abstract: This paper provides an overview about the time-linearized analysis of motion-induced and gust-induced airloads with the next-generation CFD solver framework CODA. Two approaches for obtaining time-linearized airloads are presented: the linear frequency domain solver which solves the linearized discretized RANS equations for the time-linearized response, and a system identification method which obtains the time-linearized aerodynamic response from nonlinear time-accurate simulations. Both methods are applied for typical two-dimensional and three-dimensional test cases including the NACA 64A010 airfoil, the AGARD LANN wing and the NASA CRM transport aircraft model employing pitching oscillations and sinusoidal gust encounter. By comparison of both approaches, the consistent and accurate implementation of the LFD solver and the time-accurate integration scheme in the CODA framework for time-linearized forced motion and gust encounter simulations is verified.

1 INTRODUCTION

Computational fluid dynamics (CFD) methods based on the Reynolds-averaged Navier-Stokes (RANS) equations have become essential tools in aircraft design for assessing loads and stability due to their ability to account for nonlinearities in modelling transonic or separated flow. However, the vast parameter space investigated in aircraft design and the high computational effort of unsteady RANS-based CFD methods limits their application. Time-linearized airloads provide a cost-effective way to incorporate unsteady RANS methods in industrial applications, while retaining the fidelity of the RANS flow solution [1].

The time-linearized airloads are obtained from the aerodynamic response due to small-amplitude harmonic perturbations around a steady flow. This method is well suited for flutter onset predictions, where the linear, time-invariant dynamics of the aeroelastic system is relevant. For gust loads prediction, time-linearized airloads can offer mostly conservative estimates [2] and enhance the industrial loads process [3].

The time-linearized aerodynamic response can directly be solved in the frequency domain after linearization of the discretized RANS equations under the assumption of harmonic perturbations. This linear frequency domain (LFD) solver requires the construction of the Jacobian matrix of the discretized fluxes and utilizing a robust linear solver [4]. An alternative method is to use the technique of system identification where the steady flow is perturbed by a forced excitation of very small amplitude. Since this response in the time domain can then be considered linear, the frequency response can be derived from the resulting data [5, 6].

The next-generation CFD framework CODA [7] comes with improved capabilities regarding the implementation and modelling of the discretized flow. In particular, through the use of automatic differentiation (AD) of the implemented equations, the flux Jacobian matrix required for the LFD solver can be evaluated directly. This eliminates limitations from previous hand-differentiated approaches [8] and expands the features of the LFD solver. Especially, more turbulence models than variants of the one-equation Spalart-Allmaras (SA) [9] like Menter's two-equation SST k-ω model [10] are available. Furthermore, CODA is fully coupled with the linear algebra framework Spliss [11], providing access to a range of advanced linear solvers such as preconditioned GMRES [12]. The capabilities of CODA's LFD solver have been demonstrated and validated by Vevek et al. [13] through comparison with the DLR TAU-Code [14] and experimental data.

The objective of this paper is to utilize both considered approaches for obtaining time-linearized airloads in a unified setting, which allows to verify the consistent implementation of CODA's LFD solver and the unsteady time-integration scheme with moving meshes. The latter being the only necessity for the system identification method. The paper is organized as follows. In Sec. 2, the two approaches for retrieving the time-linearized airloads and their application in the CODA framework are described. In Sec. 3, the results obtained by both approaches are compared for pitching oscillations and gust encounter of the NACA 64A010 airfoil, pitching oscillations of the AGARD LANN wing, and gust encounter of NASA Common Research Model (CRM). Sec. 3 concludes this paper with a summary and outlook.

2 BACKGROUND AND METHOD

The aeroelastic governing equations can be formulated as the second-order, linear equations of motion coupled with the aerodynamic forces. This equation can be transformed in terms of generalized coordinates by the matrix of structural eigenvectors $\mathbf{\Phi}_{gh}$ as well as transformed into the frequency domain by assuming harmonic modal displacements with amplitudes $\hat{\mathbf{q}}$ around a steady state:

$$-\omega^2 \mathbf{M}_{hh}\hat{\mathbf{q}}(\omega) + \mathbf{K}_{hh}\hat{\mathbf{q}}(\omega) = \mathbf{\Phi}_{gh}^T \mathbf{H}_{ga}\hat{\mathbf{f}}_a = \hat{\mathbf{f}}(\omega) = \mathbf{A}(\omega)\hat{\mathbf{q}}(\omega), \tag{1}$$

where $\mathbf{M}_{hh}$ and $\mathbf{K}_{hh}$ are the generalized mass and stiffness matrices. This gives rise to the time-linearized aerodynamic force distribution $\hat{\mathbf{f}}_a$, which can be projected onto the generalized coordinates by the matrix of structural eigenvectors transferred to the aerodynamic coordinates with the spline matrix $\mathbf{H}_{ga}$. The generalized aerodynamic force (GAF) matrix $\mathbf{A}(\omega)$ gathers the aerodynamic responses due to oscillating individual mode shapes enabling the superposition of the individual force contributions. Therefore, the computation of the time-linearized aerodynamic force distribution and subsequently the generalized aerodynamic force around a steady flow field for a set of mode shapes is necessary for the time-linearized analysis and loads recovery. Moreover, the GAF matrix can be extended to include the contributions of sinusoidal gusts [2], where the gust field is introduced as additional negative grid velocities [15]. In the

aeroelastic context, the angular frequency ω is normalized to the so-called reduced frequency:

$$\omega^* = \omega \frac{L}{U_\infty}, \tag{2}$$

with a characteristic length L and the free-stream velocity U_∞.

In CODA, the integral forces are obtained by integration of the face boundary flux over the wall boundaries [16]. For consistency, the cell-local quantities of the pressure coefficient c_p and vector of skin friction coefficient $\mathbf{c}_f$ are obtained similarly from the face boundary flux. Hence, the aerodynamic force acting on a surface cell can be determined by

$$\mathbf{f}_a = q_\infty \left(c_p \mathbf{n} a + \mathbf{c}_f a \right) \tag{3}$$

where $\mathbf{n}$ is the normal vector of the surface cell, a the surface cell area and $q_\infty = \rho_\infty U_\infty^2/2$ is the free-stream dynamic pressure. By providing the displacement vectors of a structural mode shape at the surface cell centers, the forces can be projected onto the generalized coordinates yielding the generalized aerodynamic force.

For both the LFD solver and the system identification, it is necessary to obtain the steady state of the finite-volume discretized flow with CODA first. The steady flow solution is obtained by employing the linearized implicit Euler method with cell-local time stepping, determined by the CFL number. The nonlinear iterations are solved by a Newton-Krylov solver, where the resulting linear systems are solved by a preconditioned GMRES up to a requested reduction in linear residual before updating the flow solution for the next iteration. The adoption of an implicit solution scheme facilitates large local time steps which is achieved by a employing a switched evolution relaxation (SER). SER increases or decreases the CFL number after every iteration based on the current residual reduction [17]. For all considered cases a nonlinear residual reduction of 10^{-10} is achieved.

2.1 System identification method

The method of system identification relies on performing nonlinear time marching simulations accurately representing the flow dynamics resulting from external excitation. By choosing very small excitation amplitudes, the linear, time-invariant response is virtually found as the nonlinear time domain response. This allows to compute the time-linearized response as the transfer function between the Fourier transformed excitation signal δ and the response signal. Using the example of the pressure coefficient, this can be written as

$$\hat{c}_p(\omega) = \frac{\mathrm{DFT}(c_p(t) - \overline{c}_p)}{\mathrm{DFT}(\delta(t))}, \tag{4}$$

where the discrete Fourier transformation (DFT) is computed by the Fast Fourier Transformation algorithm [18]. Subtracting the steady state from the time signal, normalizes the zeroth frequency content. In the linear region, the discrete spectrum of the excitation signal determines the obtained spectrum of the time-linearized response. Hence, a short-time pulse excitation results in a broadband response, where the time step size determines the maximum obtainable frequency according to the Nyquist theorem. The total simulation period determines the minimum frequency and thus, the frequency resolution. A single frequency can be obtained by exciting with a pure sinusoidal signal and computing the transfer function for a single period of this frequency. However, the validity of the assumed linearity must be ensured by an amplitude study.

For performing unsteady time-domain simulations, CODA provides a family of diagonally implicit Runge-Kutta (DIRK) time integration schemes, which enables time-accurate simulation in a dual time manner by nesting the linearized implicit Euler method with local time stepping as employed for the steady flow solution. In this work, a two-stage second-order scheme [19] is used. The accuracy of the time integration is determined by both the time step size and the convergence of the inner nonlinear iterations. To minimize the computational effort, the number of inner iterations is limited by either a fixed number of iterations or by an achieved nonlinear residual reduction. Moreover, the matrix-vector products with the flux Jacobian matrix in the inner Newton-Krylov solver are computed with one-sided finite differences. This results in a performance gain which can become quite significant when computing hundreds of time steps. The inner GMRES is preconditioned with an incomplete lower-upper (ILU) factorization with zero fill-in [20] and stopped after a linear residual reduction of 0.1.

2.2 Linear frequency domain solver

The LFD solver is derived by the linearization of the RANS equations in semi-discretized form, which can be written in terms of the state vector $\mathbf{W}$ of the conservative variables for the finite-volume discretized fluid as

$$\frac{\mathrm{d}(\mathbf{MW})}{\mathrm{d}t} + \mathbf{R}(\mathbf{W}, \mathbf{x}, \mathbf{v}) = \mathbf{0}, \tag{5}$$

where $\mathbf{R}$ is the residual vector accounting for the the inviscid and viscous fluxes, $\mathbf{M}$ is the integration matrix consisting of the discretized cell volumes, $\mathbf{x}$ are the grid node coordinates and $\mathbf{v}$ is the vector of grid node velocities. The linearization entails expanding $\mathbf{R}(\mathbf{W}, \mathbf{x}, \mathbf{v})$ in the Taylor series of first order around the steady state $\overline{\mathbf{W}}$, $\overline{\mathbf{x}}$ and $\overline{\mathbf{v}}$, with $\overline{\mathbf{R}}$ approximately zero. Under the assumption of harmonic excitation of angular frequency ω with amplitudes $\hat{\mathbf{x}}$, $\hat{\mathbf{v}}$ resulting in a harmonic response of amplitude $\hat{\mathbf{W}}$, the linearized discrete RANS equation can be written as a linear system of equations for the unknowns $\hat{\mathbf{W}}$ as

$$\left(\mathrm{i}\omega\mathbf{I} + \partial_{\mathbf{W}}\widetilde{\mathbf{R}}(\overline{\mathbf{W}}, \overline{\mathbf{x}}, \overline{\mathbf{v}})\right)\hat{\mathbf{W}} = -\overline{\mathbf{M}}^{-1}\partial_{\mathbf{x}}(\mathbf{M}\widetilde{\mathbf{R}})(\overline{\mathbf{W}}, \overline{\mathbf{x}}, \overline{\mathbf{v}})\hat{\mathbf{x}} - \partial_{\mathbf{v}}\widetilde{\mathbf{R}}(\overline{\mathbf{W}}, \overline{\mathbf{x}}, \overline{\mathbf{v}})\hat{\mathbf{v}}, \tag{6}$$

where $\widetilde{\mathbf{R}} = \mathbf{M}^{-1}\mathbf{R}$ is normalized by the cell volumes as it is employed in CODA. The left-hand side includes the flux Jacobian matrix $\partial_{\mathbf{W}}\widetilde{\mathbf{R}}(\overline{\mathbf{W}}, \overline{\mathbf{x}}, \overline{\mathbf{v}})$, which is available by AD. Moreover, $\widetilde{\mathbf{R}}$ accounts for the additional flux from cell volume changes resulting from grid node velocities by implementing a geometric conservation law.

The right-hand side is evaluated as approximations to the directional derivatives by the central finite differences

$$\partial_{\mathbf{x}}(\mathbf{M}\widetilde{\mathbf{R}})(\overline{\mathbf{W}}, \overline{\mathbf{x}}, \overline{\mathbf{v}})\hat{\mathbf{x}} \approx \frac{1}{2\varepsilon}\left(\mathbf{M}_{+\varepsilon}\widetilde{\mathbf{R}}(\overline{\mathbf{W}}, \overline{\mathbf{x}} + \varepsilon\hat{\mathbf{x}}, \overline{\mathbf{v}}) - \mathbf{M}_{-\varepsilon}\widetilde{\mathbf{R}}(\overline{\mathbf{W}}, \overline{\mathbf{x}} - \varepsilon\hat{\mathbf{x}}, \overline{\mathbf{v}})\right), \tag{7}$$

$$\partial_{\mathbf{v}}\widetilde{\mathbf{R}}(\overline{\mathbf{W}}, \overline{\mathbf{x}}, \overline{\mathbf{v}})\hat{\mathbf{v}} \approx \frac{1}{2\varepsilon}\left(\widetilde{\mathbf{R}}(\overline{\mathbf{W}}, \overline{\mathbf{x}}, \overline{\mathbf{v}} + \varepsilon\hat{\mathbf{v}}) - \widetilde{\mathbf{R}}(\overline{\mathbf{W}}, \overline{\mathbf{x}}, \overline{\mathbf{v}} - \varepsilon\hat{\mathbf{v}})\right), \tag{8}$$

with $\mathbf{M}_{\pm\varepsilon} = \mathbf{M}(\overline{\mathbf{x}} \pm \varepsilon\hat{\mathbf{x}})$ being the cell volumes of the deformed mesh.

The amplitudes $\hat{\mathbf{x}}$ and $\hat{\mathbf{v}}$ are defined by the type of excitation. If the time-linearized response to a mode shape is computed, $\hat{\mathbf{x}}$ is the vector of displacements and the grid velocities are the time derivatives of the grid coordinates: $\hat{\mathbf{v}} = \mathrm{i}\omega\hat{\mathbf{x}}$. In the case of gust encounter, the grid does not deform, $\hat{\mathbf{x}} = 0$, and the grid velocities account for the sinusoidal gust field, see [6], resulting to

$$\hat{\mathbf{v}} = -\hat{\mathbf{v}}_{gust}\exp\left(\mathrm{i}\omega\frac{\mathbf{x}_0 - \overline{\mathbf{x}}}{U_\infty}\right), \tag{9}$$

with the gust vector $\hat{\mathbf{v}}_{gust}$ defining the direction and amplitude of the gust field, and the gust reference position $\mathbf{x}_0$ determining the phase shift.

In this work, the linear system of Eq. 6 is solved, with a restarted GMRES using the ILU preconditioner [20] without fill-in reaching a reduction in the linear residual of 10^{-8}. The required matrix-vector products with the flux Jacobian matrix are computed with the memory-efficient AD variant. By a change of variables, the obtained amplitudes of the conservative variables are transformed to amplitudes of the primitive variables [21] from which further time-linearized quantities can be obtained. Hence, for computing the time-linearized pressure coefficient $\hat{c}_p$, a small-amplitude perturbed steady flow state is constructed which enables the computation of the pressure coefficient by the face boundary flux as employed in CODA. From this, $\hat{c}_p$ is obtained by a one-sided finite difference with a step size of 10^{-3}. Following Eq. 3, while neglecting the viscous force terms, the time-linearized force acting on a surface cell can be written as

$$\hat{\mathbf{f}}_a = q_\infty \left(\hat{c}_p \mathbf{n} a + \overline{c}_p \partial_{\mathbf{x}} (\mathbf{n} a) \hat{\mathbf{x}} \right), \tag{10}$$

where the second term accounts for the harmonic contribution of the surface-area weighted normal vector in case of grid deformation. The change in the surface-area weighted normal vector is again approximated by a one-sided finite difference to

$$\partial_{\mathbf{x}} (\mathbf{n} a) \hat{\mathbf{x}} \approx \frac{1}{\varepsilon} \left(\mathbf{n}(\overline{\mathbf{x}} + \varepsilon \hat{\mathbf{x}}) a(\overline{\mathbf{x}} + \varepsilon \hat{\mathbf{x}}) - \mathbf{n}(\overline{\mathbf{x}}) a(\overline{\mathbf{x}}) \right). \tag{11}$$

3 RESULTS

3.1 NACA 64A010 pitching oscillations

The NACA 64A010 is a symmetrical airfoil and is a commonly used two-dimensional aeroelastic test case [4]. The flow parameters are based on the CT8 case [22] where forced sinusoidal pitching motion was experimentally performed in transonic flow.

Table 1: Flow parameters for NACA 64A010 case.

Parameter	Value
Mach number	0.8
Reynolds number	$12 \cdot 10^6$
Reference temperature	300 K
Angle of attack	0 deg
Reference length $L = c$	1 m

The computational mesh used for this analysis is a three-dimensional mesh spanning one cell perpendicular to the airfoil section. At the sides symmetry boundary conditions are applied to model two-dimensional flow. The mesh consists of a structured grid of hexahedrons resolving the boundary layer and a unstructured grid of prisms for the farfield, see Fig. 1**b**. The computational mesh comprises 21454 nodes in total.

Tab. 1 lists the flow parameters and Fig. 1**a** shows the obtained steady pressure coefficient distribution employing two different turbulence models: SA-neg [9] and SST [10]. Both cases are computed employing a second-order Roe upwinding scheme with an entropy-fix coefficient of zero and local time stepping with SER CFL ramping (ranging from 10 to 5000). The gradients are calculated by the Green-Gauss method. In case of the SST model, the two transport equations are decoupled from the mean flow and spatially discretized with first order to improve the

robustness and accuracy of the flow solution. The steady flow exhibits strong recompression shocks at the centers of the upper and lower side. Both turbulence models give almost the same results in terms of the pressure distribution with the same shock position and strength.

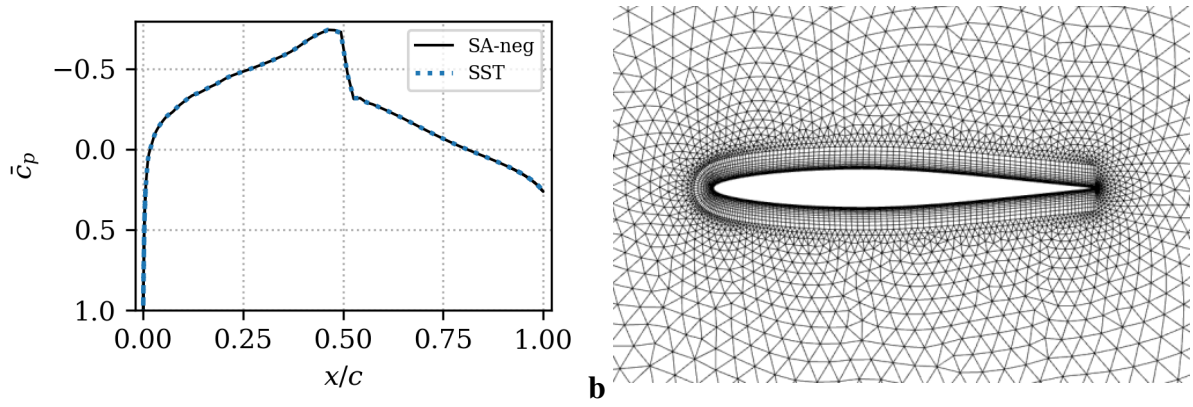

Figure 1: NACA 64A010 case (**a**) steady pressure coefficient distribution obtained with SA-neg and SST turbulence models, (**b**) near-wall mesh.

Based on the obtained steady flow fields, unsteady pitching simulations around the airfoil's quarter point are performed in the time domain and by employing the LFD solver in order to obtain the time-linearized aerodynamic responses. In the time-domain, sinusoidal pitching oscillations with varying frequencies and a broadband pulse excitation are carried out by rotating the mesh and employing a dual time-stepping to advance in physical time. The time step size is chosen by setting the number of samples per period of the pitching frequency. The sinusoidal excitations are computed with 64 samples per period, while for the broadband pulse signal a time step size of 64 samples for a reduced frequency of 1 is chosen. The inner iterations are stopped after reaching a reduction in the nonlinear residual of 10^{-5} for each stage of the DIRK scheme. For the broadband pulse computation the number of inner iterations is limited to a maximum of 10 per stage in order to avoid computational cost. This limit is reached after the pulse excitation, where the excitation signal is zero. However, the achieved residual reduction is close to the target reduction. For the inner time step size, a CFL number of 10^6 is used. The amplitude of the pitching excitations is chosen to 10^{-5} deg, which is ensured to be in the linear region. The same small amplitude is chosen for the step size ε for computing the right-hand side of the LFD equation via the finite central differences, cf. Sec. 2.2.

In the following analysis, the forces and pressure coefficients are computed as described in Sec. 2. Fig. 2 shows the excitation signals together with the dynamic lift response for the pulse and the sinusoidal excitation with a reduced frequency of 0.3. For the sinusoidal case, the lift coefficient approaches a constant sinusoidal response. Hence, each sinusoidal excitation is simulated for 5 periods to improve on the accuracy of the frequency response. Although, typically not more than 3 periods are required for an adequate accuracy, which can be determined by employing a sliding window method for computing the transfer function. For the lift coefficient due to the pulse excitation a broadband response is observed. The pulse response is simulated to achieve a resolution of reduced frequency of 0.01, which requires 3200 time steps.

Fig. 3 and Fig. 4 present the time-linearized response in terms of the lift coefficient and pressure coefficient distribution using the SA-neg and the SST model. For each model, the time-linearized response is shown obtained through broadband pulse excitation, by sinusoidal excitations of eight frequencies, and by the LFD solver for 16 frequencies. For both turbulence

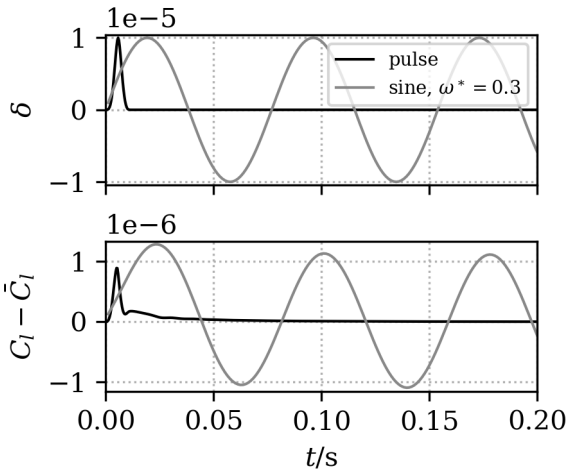

Figure 2: Time-domain response of the lift coefficient C_l for the pitching NACA 64A010 with a broadband pulse and sinusoidal excitation signal δ in degree (SA-neg).

models, excellent agreement is found in between the three employed techniques showing the accurate and consistent implementation of the nonlinear time domain and the linear frequency domain flow solvers in CODA. Moreover, there is an excellent agreement for the local quantity of the pressure coefficient. For the SST model, the same level of accuracy between the methods is achieved. In terms of the lift coefficient response no significant differences are observed between both turbulence models. However, the response in the pressure coefficient at the shock position exhibits a much stronger response for the SST model than for SA-neg. This indicates that for other integral forces like the moment coefficient differences between the models may be observed. Furthermore, it shows that the unsteady response can be different for both turbulent models, although the steady pressure coefficient distribution is very similar.

The results confirm the capability of CODA's LFD solver to work with the SST turbulence model by utilizing the AD implementation within CODA. This demonstrates the advantage of the availability of AD in a CFD framework as the SST model is not available for the LFD solver of the DLR TAU-Code.

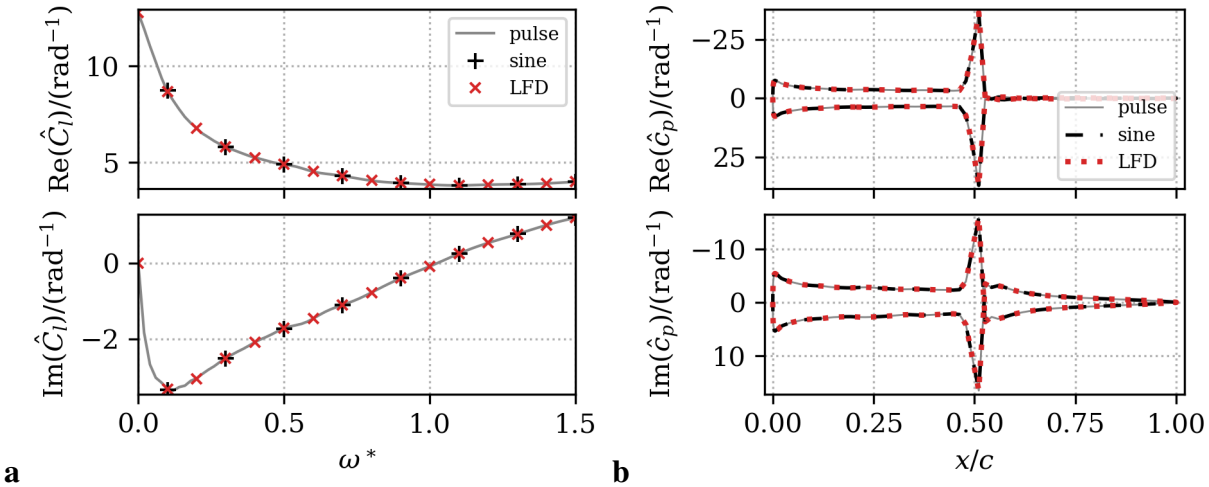

Figure 3: Frequency response with SA-neg model for the pitching NACA 64A010, obtained via a broadband pulse, sinusoidal excitation and LFD solver (**a**) of the lift coefficient $\hat{C}_l$ over reduced frequency and (**b**) the pressure coefficient distribution $\hat{c}_p$ for $\omega^* = 0.3$.

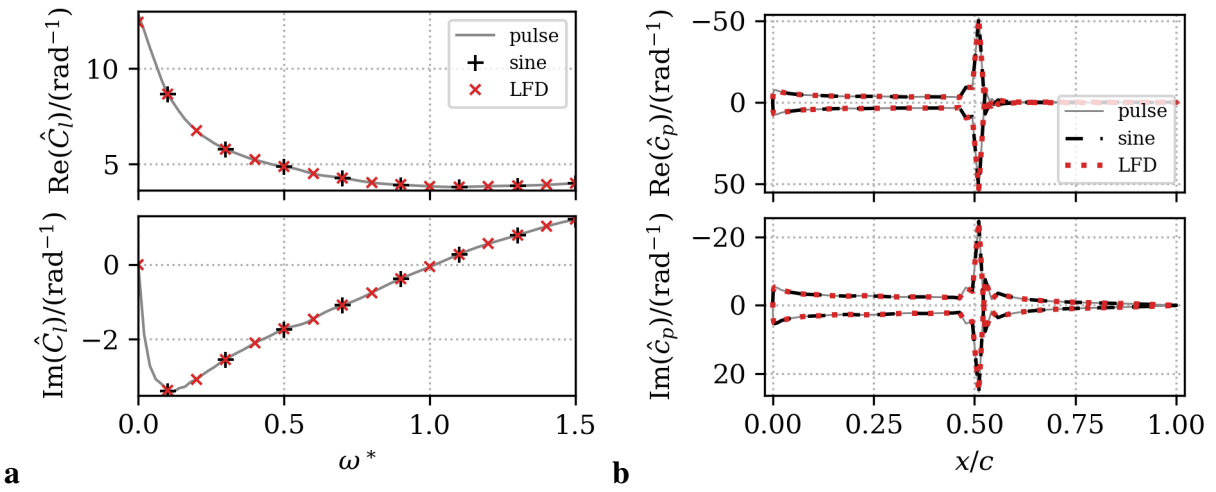

Figure 4: Frequency response with SST model for the pitching NACA 64A010, obtained via a broadband pulse, sinusoidal excitation and LFD solver (**a**) of the lift coefficient $\hat{C}_l$ over reduced frequency and (**b**) the pressure coefficient distribution $\hat{c}_p$ for $\omega^* = 0.3$.

Finally, Fig. 5 shows the comparison between CODA and DLR TAU-Code for the pitching NACA 64A010. The same computational grid is analysed with the DLR TAU-code which is a cell-vertex based finite-volume solver and here employed with the central Jameson-Schmidt-Turkel (JST) scheme [23] using the SA-neg model. The frequency response is obtained by employing the LFD solver of the DLR TAU-Code [4]. The steady pressure coefficient distribution agrees very well with CODA with small differences in the vicinity of the shock as shown in Fig. 5**a**. The shock is slightly more diffused for the TAU solution which also becomes visible by comparing the frequency response of the pressure coefficient distribution for $\omega^* = 0.3$, see Fig. 5**b**. The unsteady pressure coefficient near the shock is also more diffused and produces a lower peak amplitude. This effect is likely attributed to the coarse mesh in combination with the difference of using the Roe upwinding scheme in CODA and the JST scheme in the DLR TAU-Code.

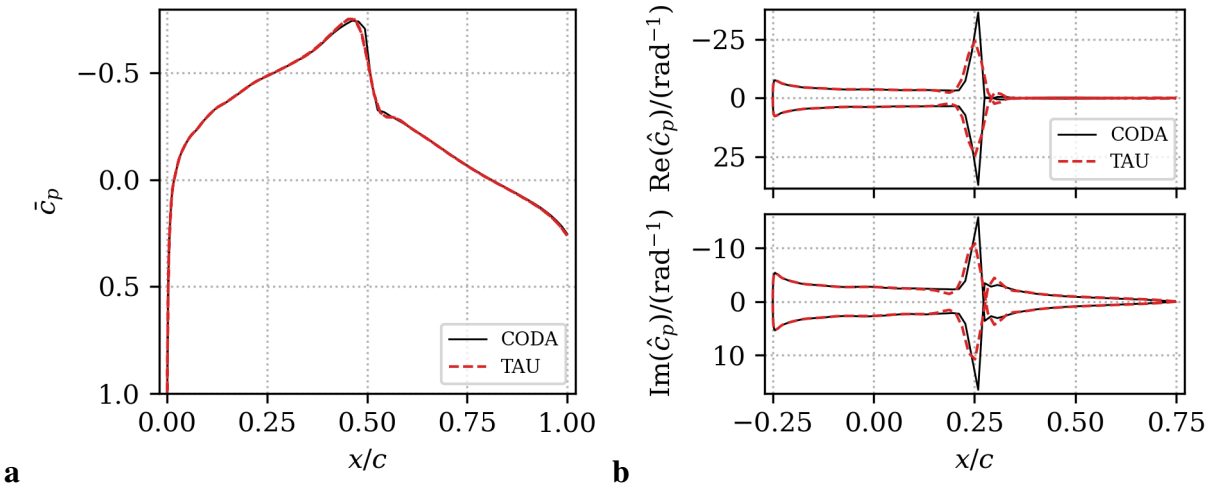

Figure 5: Comparison between CODA and DLR TAU-Code for the pitching NACA 64A010 with SA-neg (**a**) steady pressure coefficient distribution, and (**b**) pressure coefficient distribution $\hat{c}_p$ for $\omega^* = 0.3$ obtained from LFD solvers.

3.2 NACA 64A010 gust encounter

The time-linearized gust response for the NACA 64A010 is investigated in this section. This case is based on the pitching case of the previous section, Sec. 3.1, and uses the same computational grid as well as the same flow parameters. Thus, the steady flow solution for the SA-neg turbulence model can be reused in order to perform time-linearized vertical gust encounters with the LFD solver as well as in the time domain.

In the time domain, a broadband pulse excitation as well as single frequency excitations are performed with propagating gust fields which are induced every time step through the grid velocities, cf. Sec 2. The time step sizes are determined by computing 64 samples per period of the excitation frequency, which is chosen to 1 for the broadband pulse excitation. As in the pitching case, the inner iterations for each DIRK stage are stopped after a nonlinear residual reduction of 10^{-5}, while the pulse has a limit of 10 iterations. The CFL number for the inner iterations is 10^6. The amplitude of the gust field is expressed as a corresponding angle of incidence, which results from the gust's propagation velocity, typically the free-stream velocity U_∞. Hence, this angle in radian is obtained by the ratio v_{gust}/U_∞. This scaling allows to compare the obtained time-linearized gust response with the response for the pitching airfoil which are presented in radian in Sec. 3.1. For very low frequencies, both types of time-linearized response converge. The excitation amplitude is chosen to 10^{-5} rad. This is confirmed to be in the linear region by an amplitude study and the same value is taken for obtaining the right-hand side of the LFD solver via central differences.

Fig. 6 shows time-linearized gust response in terms of the lift coefficient up to a reduced frequency of 1.5 and the pressure coefficient distribution for $\omega^* = 0.3$. Likewise to the pitching case, excellent agreement is found between the solutions of the LFD solver and the results obtained from the time domain. This verifies the application of CODA's LFD solver as well as the time-accurate simulations for the time-linearized gust encounter.

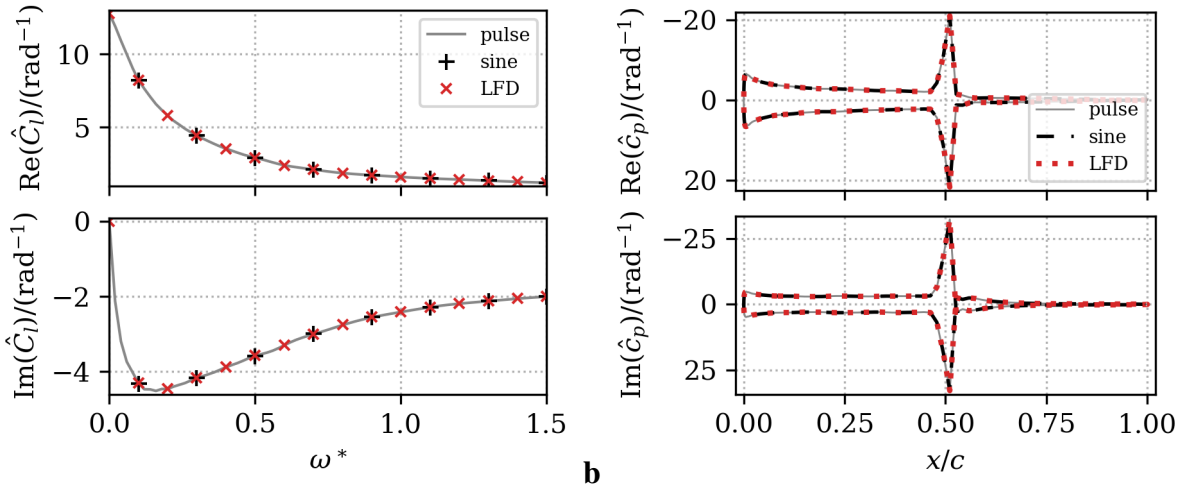

Figure 6: Frequency response with SA-neg model for the NACA 64A010 gust encounter per gust angle in radian, obtained via a broadband pulse, sinusoidal excitation and LFD solver (**a**) of the lift coefficient $\hat{C}_l$ over reduced frequency, and (**b**) the pressure coefficient distribution $\hat{c}_p$ for $\omega^* = 0.3$.

3.3 LANN wing pitching oscillations

The AGARD LANN wing [24] is a commonly used aeroelastic test case representing a tapered wing of a transport aircraft in transonic flow with a supercritical airfoil section. It is a semi-span

model with an aspect ratio of 7.92, a quarter-chord sweep angle of 25 deg, and a semi-span of $s = 1$ m. The root chord length is 0.3608 m and the mean aerodynamic chord is 0.268 m. The flow parameters investigated in this section are based on the CT5 case [24] where forced sinusoidal pitching motion around a y parallel axis was experimentally performed in transonic flow. The pitching axis is located by $x = 0.224$ m and $z = 0$ m, with the leading edge point at the wing root laying at the origin.

Table 2: Flow parameters for LANN wing case.

Parameter	Value
Mach number	0.82
Reynolds number	$5.43 \cdot 10^6$
Reference temperature	273 K
Angle of attack	0.6 deg
Reference length L	0.268 m
Reference area a_{ref}	0.2526 m^2

The computational grid, shown in Fig 7, is a hexahedron-dominant mesh with 17906 wall surface nodes and a total of 809277 grid nodes. The farfield extends in a semi-sphere around the origin with a radius of 1000 m. At the x-z plane, symmetry boundary conditions are applied. Tab. 2 lists the investigated flow parameters. The steady flow solution is computed employing a second-order Roe upwinding scheme with an entropy-fix coefficient of zero using the SA-neg turbulence model. The solution is obtained in a two-staged scenario, where initially the solution is approximated employing a constant reconstruction of the cell-face values, iterated until a nonlinear residual reduction of 10^{-3} is achieved. Subsequently, this solution is further converged with a limited linear reconstruction using a quintic spline limiter for bounding the cell gradients, which are computed by the Green-Gauss method. The solution update in each nonlinear iteration of the Newton-Krylov solver is damped employing a nonlinear positivity filter. The SER ramp is used to regulate the CFL number for the local time stepping from 2 up to $3.4 \cdot 10^5$. The final residual reduction of 10^{-10} is achieved after a total of 154 nonlinear iterations.

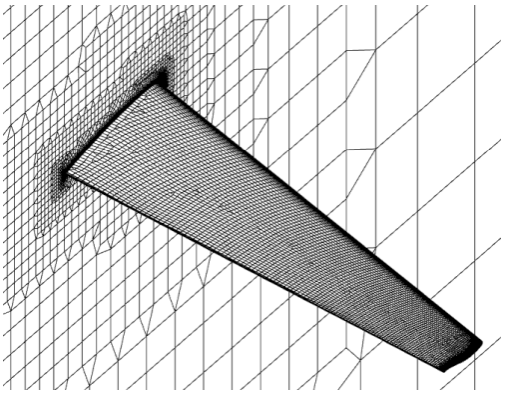

Figure 7: LANN wing computational grid

Around the steady flow solution, unsteady pitching simulations are performed in the time domain with a broadband pulse and single frequency excitations as well as by applying the LFD solver in order to obtain the time-linearized response. The pitching motion is considered by deforming the mesh with a scaled displacement field resulting from a linearized rotation around the pitch axis as only very small rotation angles are investigated. For the time-domain simula-

tions, the time step sizes result from sampling each excitation period with 64 samples, where 1 is set as the reference frequency of the broadband pulse excitation. The inner iterations are performed with a CFL number of 10^6 and each DIRK stage is stopped after reaching a nonlinear residual reduction of 10^{-3} or after 10 iterations for the pulse excitation. Within each stage, it is observed that the number of required linear iterations of the GMRES solver increases as the nonlinear residual converges, resulting in an increasing computational cost per magnitude of nonlinear residual reduction. However, for maintaining accuracy a significant reduction is required. This may be relaxed employing a smaller time step size but for the cost of an increased number of samples to be computed. The excitation amplitude is 10^{-5} deg, and the same value is used as the step size for computing the right-hand side of the LFD equation, cf. Sec. 2.2.

Fig. 8 shows the steady and unsteady pressure coefficient distributions a two span-wise sections for a pitching frequency of $\omega^* = 0.15$, which is close to the experimentally investigated 24 Hz. The first section is close to the wing root, $y/s = 0.2$. From the steady pressure distribution two recompression shocks are found on the upper side around $x/c \approx 0.2$ and close to the center. The two shocks stem from a λ-shock system which is found on the upper side of the wing [4]. At the second section, closer to the wing tip at $y = 0.65$, only a single strong shock is observed at $x/c \approx 0.35$. These shock positions are also identified by the strong peaks in the time-linearized response of the pressure coefficient distribution. The comparison between the LFD solution and the results obtained in the time domain shows excellent agreement in the unsteady pressure coefficient distribution at both span-wise sections.

Fig. 9 presents the time-linearized response in terms of generalized aerodynamic force for the pitching motion. The generalized aerodynamic force f_p is obtained by projecting the aerodynamic force distribution onto the surface displacements for the linearized pitching motion, see Sec. 2. Hence, it resembles a moment of the force distribution around the pitch axis. The time-linearized GAFs are normalized to $\hat{f}_p^* = \hat{f}_p/(q_\infty a_{ref} L)$ for a linearized pitching motion of 1 rad. As for the local quantities, excellent agreement is found between the GAFs obtained by the LFD solver and from the broadband pulse response in the time domain over the range of reduced frequencies. Only for the zeroth frequency a small deviation is observed. This results most likely from the not fully converged response for the very low frequencies through the broadband pulse excitation, since the simulation period must be long enough in order to obtain the low frequencies. In this case, 1280 samples are computed for the pulse response resulting in a frequency resolution of 0.05.

Taken together, the consistent implementation of the LFD solver and the time-accurate simulations in CODA for time-linearized pitching motion of a three-dimensional wing in transonic flow is shown.

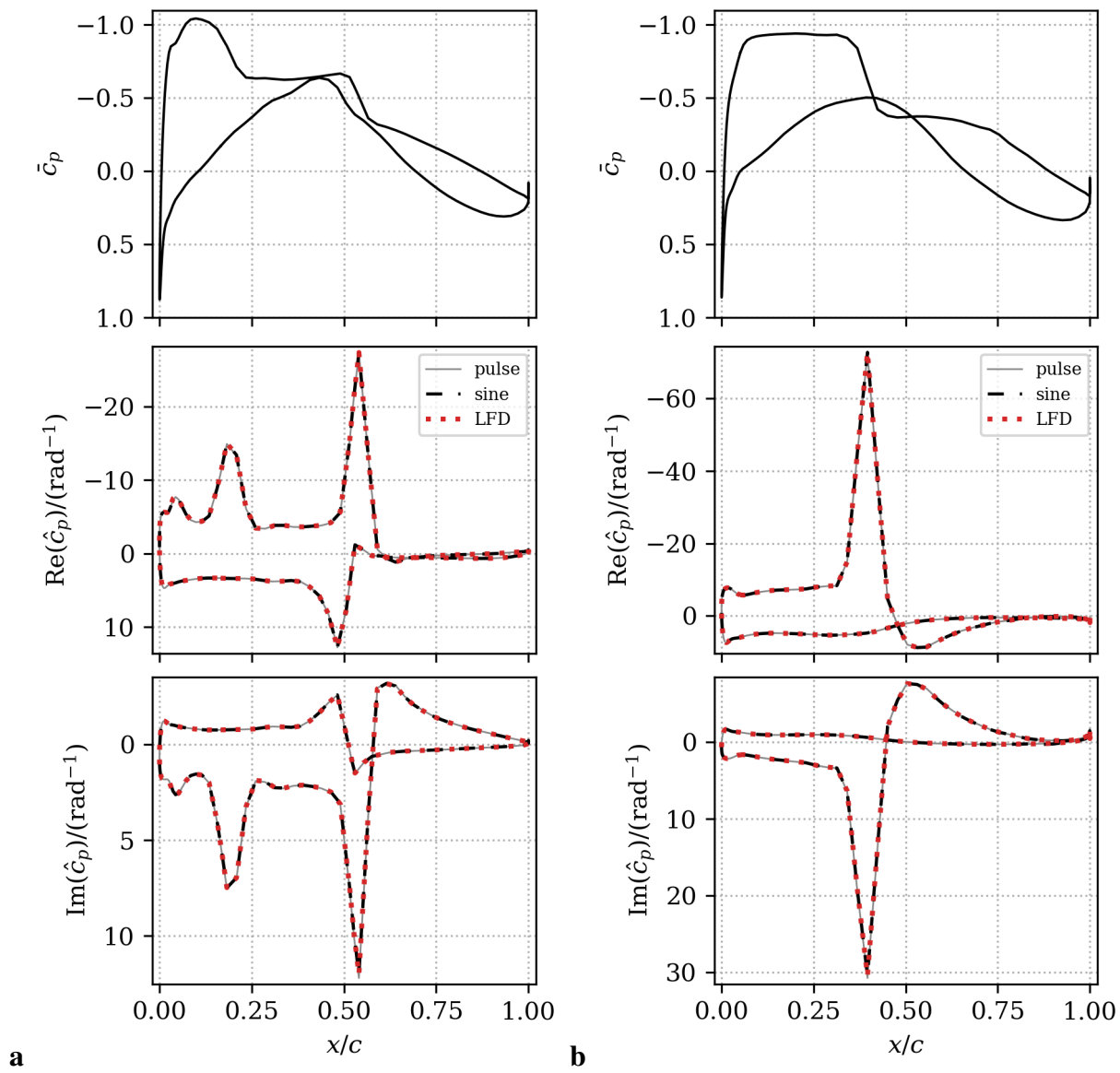

Figure 8: Steady and unsteady time-linearized pressure coefficient distribution for the LANN wing pitching oscillations with $\omega^* = 0.15$ at the span-wise sections (**a**) $y/s = 0.2$, and (**b**) $y/s = 0.65$.

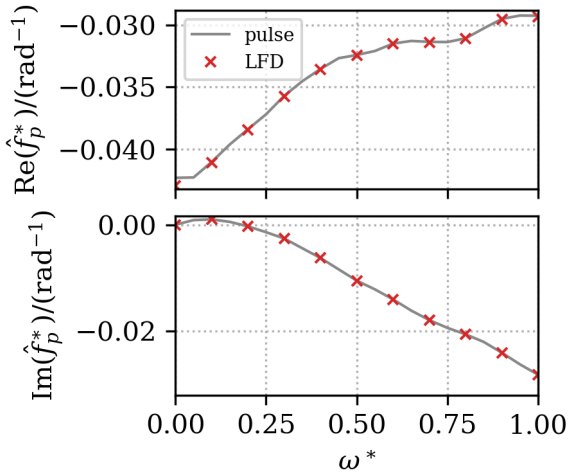

Figure 9: Normalized, time-linearized GAF for the pitching motion of the LANN wing pitching oscillations.

3.4 NASA Common Research Model gust encounter

In this section, the time-linearized gust response for the NASA Common Research Model (CRM) is investigated employing the LFD solver and a single frequency excitation in the time domain. The NASA CRM is a model of a typical civil transport aircraft designed for applied CFD validation studies [25]. The computational grid is obtained from the grid collection of the Fifth Drag Prediction Workshop [26]. The medium-sized grid L3 is taken from a series of structured grids and converted to an unstructured grid of hexahedral cells suited for CODA, see Fig. 10. The grid is a wing-body half model with 53569 surface nodes and has around $5.19 \cdot 10^6$ grid nodes in total. The grid is scaled to aircraft size with a semi-span of $s = 29.38$ m and a mean aerodynamic chord of $L = 7.00532$ m. The farfield is discretized by a semi-sphere around the aircraft with a radius of 800 m. For the x-z plane, symmetry boundary conditions are applied.

Table 3: Flow parameters for NASA CRM case.

Parameter	Value
Mach number	0.85
Reynolds number	$5 \cdot 10^6$
Reference temperature	310.9 K
Angle of attack	3 deg
Reference length L	7.00532 m

The flow parameters of the NASA CRM case are listed in Tab. 3. The steady flow solution is obtained by the second-order Roe upwinding scheme with an entropy-fix coefficient of 0.1. Likewise to the LANN wing case, a two-staged scenario is applied with an initial solution using a constant reconstruction for a residual reduction of 10^{-5}, followed by a linear cell-wise reconstruction using a quintic spline gradient limiter. The Newton-Krylov iteration updates are locally damped by a nonlinear positivity filter. The CFL number ranges from 2 up to 10^6 through the SER ramping. The final residual reduction of 10^{-10} is obtained after 114 nonlinear iterations.

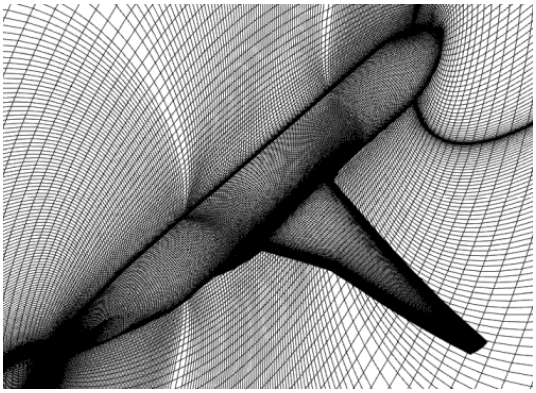

Figure 10: NASA CRM computational grid DPW5 L3

A time-linearized vertical gust encounter is performed for a reduced frequency of $\omega^* = 0.4$ which corresponds to a gust length of 110.04 m. The single frequency excitation in the time domain is simulated for 5 periods with 64 time steps per period. The CFL number for the inner iteration is set to 10^8 and each stage of the DIRK scheme is stopped after a nonlinear residual reduction of 10^{-3} or after 20 nonlinear iterations. Similar to the LANN wing case, the computational cost noticeably increases with lowering the targeted residual reduction per stage

as the number of inner iterations strongly increases. The gust amplitude and the step size for computing the right-hand side of the LFD equation is chosen to 10^{-3} m/s.

The time-linearized pressure coefficient distribution is shown in Fig. 11 for two span-wise sections of the wing together with the steady pressure coefficient distribution. For the inboard section at $y/s = 0.2$, the flow exhibits a shock in the aft part of the wing, which is also observed closer to center at the more outboard section at $y/s = 0.65$. The shock positions are then also found by the strong peaks in the time-linearized pressure coefficient distribution. Excellent agreement between the LFD solver and single frequency excitation is found for the time-linearized pressure coefficient distribution, which shows the consistent implementation of the LFD solver and the time-accurate simulations in CODA for a sinusoidal gust encounter of a typical aircraft configuration.

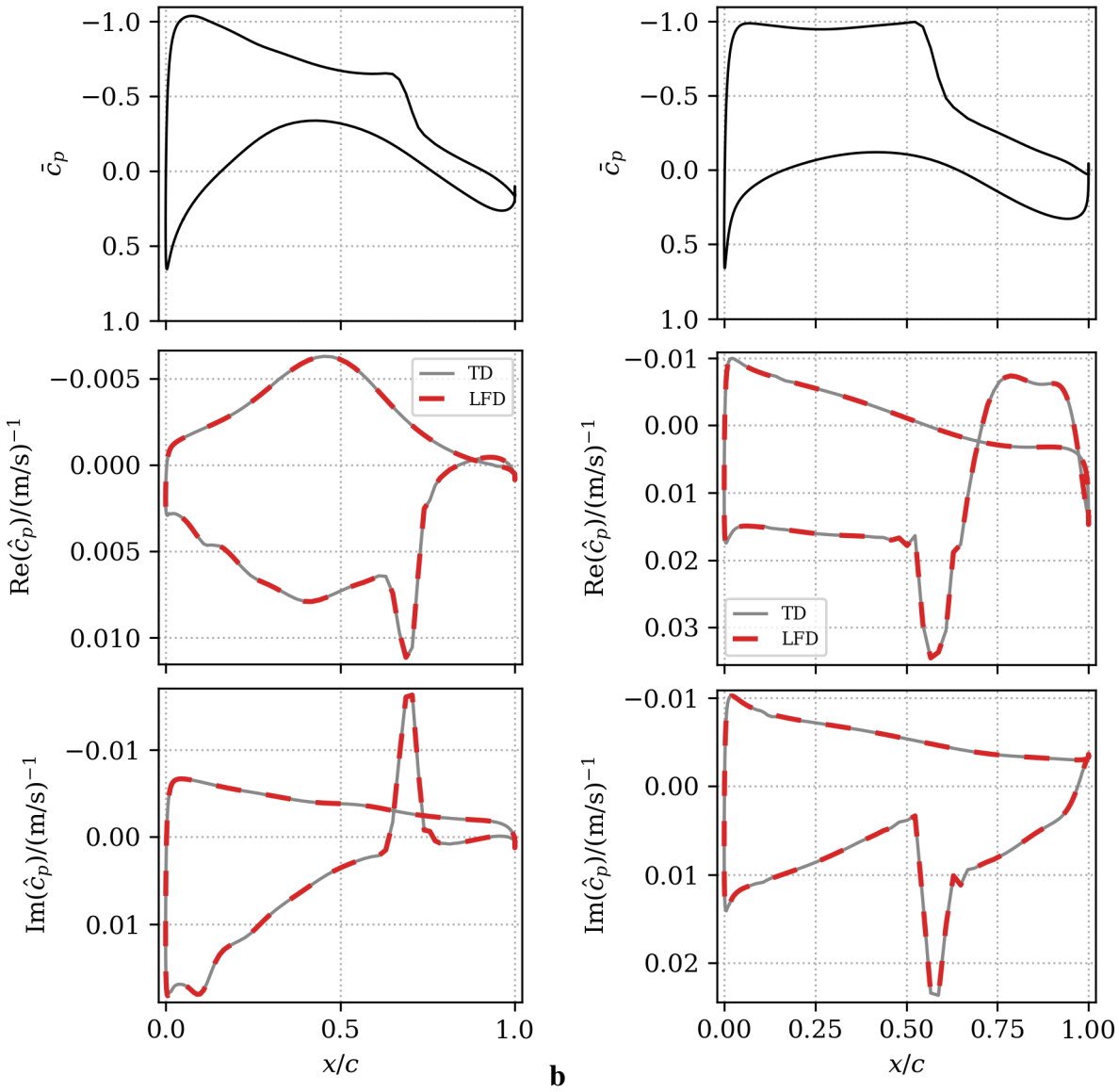

Figure 11: Steady and unsteady time-linearized pressure coefficient distribution due to a sinusoidal gust encounter in (m/s) with $\omega^* = 0.4$ at spanwise sections (**a=** $y/s = 0.2$, and (**b**) $y/s = 0.65$.

4 CONCLUSION

This paper investigates the motion-induced and gust-induced time-linearized airloads utilizing the next-generation CFD framework CODA. Two methods for obtaining time-linearized airloads are presented and applied within the CODA framework for two- and three-dimensional test cases. On the one hand, the implemented LFD solver is employed, which allows to solve the linearized discretized RANS equations by providing the necessary right-hand side for grid motion as well as gust encounter for each frequency. On the other hand, the time-linearized airloads are derived through system identification of the time-domain response due to grid motion and gust encounter with very small amplitudes. This method is demonstrated for broadband pulse signals, which yields the response for multiple frequencies, and for single-frequency sinusoidal excitation.

The presented results include pitching oscillations of the NACA 64A010 airfoil and the AGARD LANN wing. Both cases display excellent agreement in the time-linearized response between the two approaches, for local quantities like the pressure coefficient distribution as well as for integral forces. For the pitching NACA 64A010 airfoil, the same quality of agreement is found for the SST k-ω turbulence model, demonstrating the enhanced feature set of the CODA framework through AD. To the same extent, excellent agreement for the two approaches is presented for the time-linearized gust encounters for the NACA 64A010 airfoil as well as for the NASA CRM aircraft model. Taken together, the presented results demonstrate the consistent and accurate implementation of the LFD solver and the time-accurate integration scheme in CODA for time-linearized forced motion and gust encounter simulations.

Future work will address employing the LFD solver for more advanced cases like moderate flow separation. Moreover, applying the LFD solver for transition transport models and other turbulence models seems possible in the CODA framework through the AD implementation. Furthermore, increasing the efficiency of the time-accurate simulations for obtaining time-linearized responses is investigated. The two-stage second-order DIRK scheme with the nested Newton-Krylov solver employed in this work showed a significant computational demand which must be met by an efficient setup of the Newton-Krylov solver for balancing the accuracy against the computational cost. For example, DIRK schemes of higher order or Rosenbrock-Wanner methods are available for investigation in the CODA framework. Additionally, possible performance improvements from the implemented hybrid parallelization in CODA and Spliss are to be investigated for the LFD solver as well as for the time-accurate simulations.

ACKNOWLEDGMENT

This work was supported by the DLR project COANDA (CODA-Automatisierung und -Nutzbarmachung für diversifizierte Anwendungsfelder).

5 REFERENCES

[1] Chassaing, J.-C. and Gerolymos, G. (2004). Time-Linearized Time-Harmonic 3-D Navier-Stokes Shock-Capturing Schemes. In *10th AIAA/CEAS Aeroacoustics Conference*. American Institute of Aeronautics and Astronautics. ISBN 978-1-62410-071-0. doi:10.2514/6.2004-2817.

[2] Kaiser, C., Quero, D., and Nitzsche, J. (2019). Quantification of nonlinear effects in gust load prediction. In *International Forum on Aeroelasticity and Structural Dynamics 2019, IFASD 2019*.

[3] Weigold, W., Stickan, B., Travieso-Alvarez, I., et al. (2017). Linearized unsteady CFD for gust loads with TAU. In *International Forum on Aeroelasticity and Structural Dynamics, IFASD 2017*.

[4] Thormann, R. and Widhalm, M. (2013). Linear-Frequency-Domain Predictions of Dynamic-Response Data for Viscous Transonic Flows. *AIAA Journal*, 51(11), 2540–2557. ISSN 0001-1452. doi:10.2514/1.J051896.

[5] Seidel, D., Bennett, R., and Whitlow, W., Jr (1983). An exploratory study of finite difference grids for transonic unsteady aerodynamics. In *21st Aerospace Sciences Meeting*. p. 503.

[6] Kaiser, C., Thormann, R., Dimitrov, D., et al. (2015). Time-linearized analysis of motion-induced and gust-induced airloads with the DLR TAU Code. In *Deutscher Luft- und Raumfahrtkongress 2015*.

[7] Leicht, T., Jägersküpper, J., Vollmer, D., et al. (2016). DLR-Project Digital-X - Next Generation CFD Solver 'Flucs'. In *Deutscher Luft- und Raumfahrtkongress 2016*.

[8] Dwight, R., Brezillon, J., and Vollmer, D. (2006). Efficient algorithms for solution of the adjoint compressible Navier-Stokes equations with applications. In *ODAS 2006*.

[9] Allmaras, S. R. and Johnson, F. T. (2012). Modifications and clarifications for the implementation of the Spalart-Allmaras turbulence model. In *Seventh international conference on computational fluid dynamics (ICCFD7)*, vol. 1902. Big Island, HI.

[10] Menter, F. R., Kuntz, M., and Langtry, R. (2003). Ten Years of Industrial Experience with the SST Turbulence Model. *Heat and Mass Transfer*, 4.

[11] Rempke, A., Krzikalla, O., Mohnke, J., et al. (2023). Spliss: A sparse linear system solver for transparent integration of emerging HPC technologies into CFD solvers. In *Computational and Data Science Seminar*.

[12] Saad, Y. and Schultz, M. H. (1986). GMRES: A generalized minimal residual algorithm for solving nonsymmetric linear systems. *SIAM Journal on scientific and statistical computing*, 7(3), 856–869.

[13] Vevek, U. S., Timme, S., Pattinson, J., et al. (2022). Next-generation computational fluid dynamics capability for aircraft aeroelasticity and loads. In *International Forum of Aeroelasticity and Structural Dynamics, IFASD 2022*.

[14] Schwamborn, D., Gerhold, T., and Heinrich, R. (2006). The DLR TAU-Code: Recent applications in research and industry. In *ECCOMAS CFD 2006 CONFERENCE*.

[15] Singh, R. and Baeder, J. D. (1997). Direct Calculation of Three-Dimensional Indicial Lift Response Using Computational Fluid Dynamics. *Journal of Aircraft*, 34(4), 465–471. ISSN 0021-8669. doi:10.2514/2.2214.

[16] Hartmann, R. and Leicht, T. (2015). Generalized adjoint consistent treatment of wall boundary conditions for compressible flows. *Journal of Computational Physics*, 300, 754–778. ISSN 0021-9991. doi:10.1016/j.jcp.2015.07.042.

[17] Mulder, W. A. and Van Leer, B. (1985). Experiments with implicit upwind methods for the Euler equations. *Journal of Computational Physics*, 59(2), 232–246. ISSN 0021-9991. doi:10.1016/0021-9991(85)90144-5.

[18] Cooley, J. W. and Tukey, J. W. (1965). An Algorithm for the Machine Calculation of Complex Fourier Series. *Mathematics of Computation*, 19(90), 297–301. ISSN 0025-5718. doi:10.2307/2003354.

[19] Alexander, R. (1977). Diagonally Implicit Runge–Kutta Methods for Stiff O.D.E.'s. *SIAM Journal on Numerical Analysis*, 14(6), 1006–1021. doi:10.1137/0714068.

[20] McCracken, A. J., Timme, S., Badcock, K. J., et al. (2012). Accelerating convergence of the CFD linear frequency domain method by a preconditioned linear solver. In *6th European Congress on Computational Methods in Applied Sciences and Engineering*.

[21] Widhalm, M. and Thormann, R. (2017). Efficient Evaluation of Dynamic Response Data with a Linearized Frequency Domain Solver at Transonic Separated Flow Condition. In *35th AIAA Applied Aerodynamics Conference*. American Institute of Aeronautics and Astronautics. doi:10.2514/6.2017-3905.

[22] Davis, S. S. (1982). NACA 64A010 (NASA Ames model) oscillatory pitching. *Compendium of Unsteady Aerodynamic Measurements*, AGARD R-702, pp. 2–1–2–22.

[23] Jameson, A., Schmidt, W., and Turkel, E. (1981). Numerical solution of the Euler equations by finite volume methods using Runge Kutta time stepping schemes. In *14th Fluid and Plasma Dynamics Conference*, Fluid Dynamics and Co-located Conferences. American Institute of Aeronautics and Astronautics. doi:10.2514/6.1981-1259.

[24] Zwaan, R. J. (1985). LANN wing: pitching oscillation. *Compendium of Unsteady Aerodynamic Measurements, Addendum No. 1*, AGARD R-702, pp. 9–1—9–76.

[25] Vassberg, J., Dehaan, M., Rivers, M., et al. (2008). Development of a Common Research Model for Applied CFD Validation Studies. In *26th AIAA Applied Aerodynamics Conference*, Guidance, Navigation, and Control and Co-located Conferences. American Institute of Aeronautics and Astronautics. doi:10.2514/6.2008-6919.

[26] Morrison, J. (2021). DPW5 Grids and files from the Fifth Drag Prediction Workshop. `https://dpw.larc.nasa.gov/DPW5/multiblock_grids.REV01/CGNS/`. Accessed: May 2024.

COPYRIGHT STATEMENT

The authors confirm that they, and/or their company or organisation, hold copyright on all of the original material included in this paper. The authors also confirm that they have obtained permission from the copyright holder of any third-party material included in this paper to publish it as part of their paper. The authors confirm that they give permission, or have obtained permission from the copyright holder of this paper, for the publication and public distribution of this paper as part of the IFASD 2024 proceedings or as individual off-prints from the proceedings.